International Journal of u- and e- Service, Science and Technology
Vol.9, No. 10 (2016), pp.187-198
http://dx.doi.org/10.14257/ijunesst.2016.9.10.18

An Level Set Evolution Morphology Based Segmentation of Lung Nodules and False Nodule Elimination by 3D Centroid Shift and Frequency Domain DC Constant Analysis

Senthilkumar Krishnamurthy[1*], Ganesh Narasimhan[2] and Umamaheswari Rengasamy[3]

[1]*Information and Communication Engineering, Anna University, India.*
[2]*Electronics and Communication Engineering, Saveetha Engineering College, India*
[3]*Electrical and Electronics Engineering, Velammal Engineering College, India*
[1]*tkseneee@gmail.com*

Abstract

A Level Set Evolution with Morphology (LSEM) based segmentation algorithm is proposed in this work to segment all the possible lung nodules from a series of CT scan images. All the segmented nodule candidates were not cancerous in nature. Initially the vessels and calcifications were also segmented as nodule candidates. The structural feature analysis was carried out to remove the vessels. The nodules with more centroid shift in the consecutive slices were eliminated since malignant nodule's resultant position did not usually deviate. The calcifications were eliminated by frequency domain analysis. DC constant of nodule candidates were computed in frequency domain. The nodule candidates with high DC constant value could be the calcifications as the calcification patterns were homogeneous in nature. This algorithm was applied on a database of 40 patient cases with 58 malignant nodules. The algorithms proposed in this paper precisely detected 55 malignant nodules and failed to detect 3 with a sensitivity of 95%. Further, this algorithm correctly eliminated 778 tissue clusters that were initially segmented as nodules, however, 79 non-malignant tissue clusters were detected as malignant nodules. Therefore, the false positive of this algorithm was 1.98 per patient.

Keywords: *Cancer detection, Computed Tomography, Image segmentation, Medical diagnostic imaging, Level Set Evolution*

1. Introduction

Lung cancer is the uncontrolled growth of an abnormal tissue in the lung. The most commonly diagnosed cancer in the world is lung cancer (1.61 million, 12.7% of total). The World Health Organization (WHO) report says that 7.6 million(13% of all global deaths) deaths globally each year are caused by cancer, in which lung cancer lead to more deaths than all other cancers [1]. The risk of cancer is 20:1 for smokers vs. non-smokers. A quarter of the cigarette or beedi smokers in India would be killed by tobacco at the ages of 25-69 years, losing 20 years of life expectancy. Non-smoking of lung cancer cases are often attributed to a combination of genetic factors, radon gas, asbestos, pesticides and air pollution including passive and static smoking.

The diagnosis of lung cancer at early stage is critical and uncertain as the physicians direct the patient to undergo biopsy only after analyzing the multiple lung CT scans taken between a time interval of 6 to 18 months [2-3]. Nowadays, although advanced imaging techniques such as computed tomography (CT) scanning that precisely capture the images

*Corresponding Author

ISSN: 2005-4246 IJUNESST

of lung are available, finding the cancerous nodules is still a challenging task for physicians. CT scan of lung produces continuous cross-sectional images, and to confirm the cancerous nature of lung, it is essential to analyze every cross section. The radiologist needs to put extra efforts to analyze each cross-sectional image of lung and hence there is high probability of an error. The development of computer-aided diagnostic (CAD) tools will help physicians to more accurately analyze the CT scan images by reducing the image reading time.

The pixel intensity based lung nodule segmentation has been used to segment lung nodules in many studies [4-7]. In these works the threshold values were manually selected based on the CT technology and X-ray dose. Also the threshold based segmentations methods need to be followed by excessive morphological processing to segment the nodules precisely. Some literatures focused on Model based template matching methods to segment the lung nodule [8-10], but template matching techniques produce more false positives. The 2D neighbor pixels difference based region grow algorithms was also used to segment the lung nodules, but generally 2D lung nodule segmentation algorithms shows more false positive results than the 3D analysis. Hence 3D analysis is used to reduce false positives. The work implemented by Alilou M *et. al.,* [11] mainly focused on 3D structural visualization of lung nodules which produced 3.9 false positives /patient. The work published by Demir O and Yilmaz C [12] dealing with the texture 3D model of lung nodules which resulted in a false positive of 2.45/patient. The work published by Lin Lu *et. al.,* [13] using a complex hybrid model for nodule segmentation and classification, which resulted in a false positive of 3.13/patient. The genetic and fuzzy rule based algorithm proposed by Ozekes *et. al.,* [14] results in 100 percent sensitivity but with the cost of 13.4 false positives per patient.

In this work we proposed active contour based lung nodule segmentation technique followed by false nodules (vessel and calcification) elimination through 3D structural and frequency domain features. Nodules are the clusters of tissue in the parenchyma of lung. These nodules are the initial indicator to detect the lung cancer from CT scan. This work also concentrates on proper pre-processing strategy which makes the segmentation and feature extraction process reliable.

1.1. Database

LIDC (Lung Image Database Consortium) and lung images collected from Bharat scans, Chennai, India is used in this work. LIDC is the public open access online database [15]. The algorithms developed in this paper are tested on 40 different patient images (20 from LIDC and 20 from Bharat scans) and the results are satisfactory. LIDC database is provided with four radiologist ground truth report. Each image has a size of 512 × 512 inch with 16-bit gray resolution and pixel spacing of 0.76 mm in both x and y direction.

2. Pre-Processing of Lung CT Image

Computer Tomography scans are the series of collection of X-ray images. The X-ray incident on the human body will attenuate based on the attenuation coefficient of different organ's cells inside the body. These attenuated X-ray values are detected and calibrated by detectors present inside the CT machine. The CT technology is evolved rapidly in last three decades in terms good resolution and speed. The lung CT images are generally recorded in DICOM format. DICOM format images contain its pixel value in signed integer 16 bit format or unsigned integer 16 bit format. The tag information of DICOM images will tell all the information regarding CT machine technology used and patient information. Confidential information such patient data has been removed by accessing the appropriate DICOM tags before processing.

2.1. Normalization of lung CT Image

In this work the DICOM format lung CT images are normalized to unsigned 16 bit integer from signed 16 bit integer, which makes the development of image enhancement algorithms easier. The original and normalized CT images with its histograms are shown in the Figure 1.

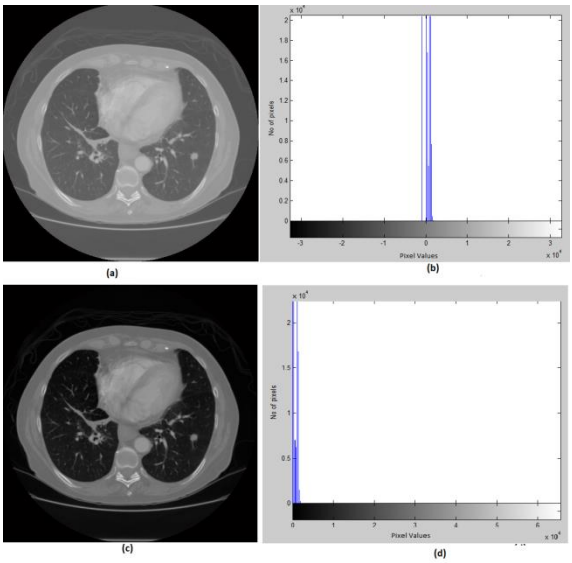

Figure 1. (a)16-Bit Signed DICOM Format Lung CT, (b)16-Bit Signed Format Histogram, (c)16-Bit Unsigned DICOM Format Lung CT, (d)16-Bit Unsigned Format Histogram

2.2. Lung CT Image Enhancement

The CT machine technology is evolved rapidly in last two decade with high tech multi X-ray detectors. Also many advanced reconstruction algorithms were developed to produce a noise free CT images. Even though lung CT image is not corrupted with much of noise, it is essential to improve the visible quality of it as the density variation of different lung region is not sharp. Density variations in the object being imaged that interfere with the diagnosis are sometimes referred to as structural "noise" or structural clutter. In standard radiography a large amount of structural clutter is produced by the superposition of various anatomic structures, for example, the image of rib bones overlaps that of the lung in a standard chest radiograph.

In this work we used customized histogram specification technique to enhance the nodules and vessels inside the lung parenchyma region. The muscle, heart and bone regions in the lung CT image are not used to diagnose the lung cancer. The region which is the primary indicator for identifying the lung cancer is 'lung nodules'. Some time wrongly the vessels inside lung parenchyma region also may be wrongly identified as lung nodules. Hence it is necessary to focus both nodules and vessels to identify the lung cancer accurately.

The lung nodule candidates inside the lung parenchyma are in between the intensity level of 600 to 1500 in unsigned 16 bit DICOM format image. The histogram equalization has been performed only on the pixels which are in this range to enhance the 'nodules'. Hence this process is known as histogram specification [16]. The applied steps for lung nodule customized histogram specification as follows

1. The total number of pixels corresponding to the each gray level from 600 to 1500 are determined.

$$c(k) = \sum_{i=600}^{1500} [f(x,y) == i] \quad (1)$$

2. The probability of each pixels in this range has been computed by dividing each pixel occurrence by the total number of pixels.

$$p(k) = \sum_{k=1}^{L} c(k)/N \quad (2)$$

where L =length of c(k) and N = total number of pixels in an image

3. Cumulative probability distribution has been computed by adding the probability of occurrences computed in the previous step.

cdf(1) = p(1)

cdf(k+1) = p(k-1) + p(k) (3)

4. Normalizing the cumulative distribution by multiplying it with the maximum pixel value of the lung CT image.

ncdf(k) = cdf(k)*max(f(x,y)) (4)

5. Redistributing the new normalized gray values obtained in the last step in place of original image pixel positions. The same steps are repeated for the intensity level of 350 to 650 to enhance the vessels inside the lung parenchyma.

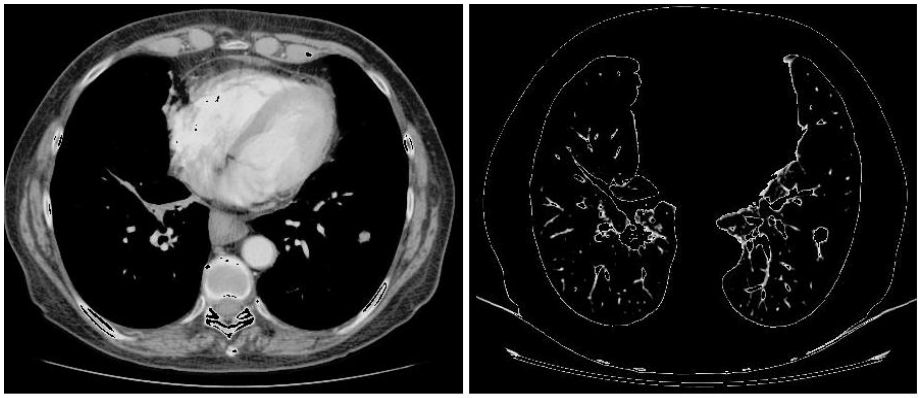

Figure 2. (a) Lung CT Image with Enhanced Nodule Candidates, (b) Lung CT Image with Enhanced Vessels

3. Level Set Evolution with Morphology (LSEM) based Segmentation

The Level Set technique is a powerful tool to segment the region of interest from an Image. Initially, Active Contours were used by Kass [17], in which the curves explicitly move to extract the region of interest in an image. In the active contour model, the selected points on the initial curve (at t=0) are moved with the velocity in the normal direction. The curve deformation in this active contour mode depends on how many points we choose. More points lead to instability, and fewer points lead to an incorrect and deformable shape in the curve. To overcome this drawback, the Level Set proposed by Osher and Sethian [18] implicitly represents the curve by the zero level of high dimensional function.

The implementation of the Level Set algorithm has three fundamental steps:

1.Initialization of Curve function φ(x,y)
2.Evolution of curve
3.Stopping condition for curve evolution

The curve can be mathematically defined as:

$$C(p)= \{(x,y) \mid \varphi(x,y) =0\} \quad (5)$$

The point p (x,y) canbe included inthe curve if the function φ(x,y) = 0. The function φ(x,y) >0 inside the curve and φ(x,y) <0 outside the curve.

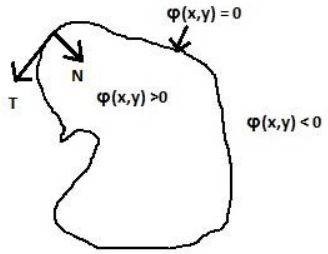

Figure 3. Level Set Function

Generally, the initial curve function can be just a rectangle, which needs to evolve consecutively to deform in such a way to fit in to the region of interest. To evolve the curve, it is essential to compute the velocity and curvature. The deformation/evolution of curve will move in the normal direction, therefore, the velocity should be defined in the normal direction. The curve also has velocity in tangential direction, but the velocity in the tangential direction doesn't change the shape of the curve. Normal and tangent component of φ is defined as:

$$\vec{N} = -\frac{\nabla\varphi}{|\nabla\varphi|} \quad (6)$$

$$\vec{T} = \frac{\vec{\nabla}\varphi}{|\nabla\varphi|} \quad (7)$$

∇φ is gradient of the curve that gives the maximum rate of change. The gradient along the curve, in the tangent of gradient is zero along the curve, which is known as Level set.

$\langle\frac{\nabla\phi}{|\nabla\phi|}, T\rangle = 0$ ---> $\frac{\nabla\phi}{|\nabla\phi|}$ is perpendicular to T.

The curvature is the second order differentiation of the curve C in the normal direction.

$$Css=k\vec{n} \quad (8)$$

where curvature $k=div\ (\frac{\nabla\phi}{|\nabla\phi|})$

The velocity of deformation of initial curve is the first order differentiation of curve in the normal direction.

$$\frac{dC}{dt} = V\vec{N} \quad (9)$$

Change of curve function with Velocity V is expressed as:

$$\frac{d\varphi}{dt} = V|\nabla\varphi| \quad (10)$$

The evolution of the curve needs to be stopped once the curve fits the region of interest. The condition to stop the curve deformation is modeled as shown below:

$$\frac{dC}{dt} = (g(x,y)k - \{\nabla g(x,y), \vec{n}\})\ \vec{n} \quad (11)$$

where $(g(x,y)k - \{\nabla g(x,y), \vec{n}\})$ is nothing but velocity V, which needs to become zero to stop deformation / curve evolution.

$$g(x,y) = \frac{1}{\nabla I} \quad (12)$$

where ∇I is the gradient of the Image. The gradient of an image is the rate of change of the image pixel values. For a smooth portion of the image the gradient(rate of change of pixel values) is decreased and at edges the rate of change is increased, *i.e.*, gradient is greater. The function g is minimal when the gradient of the image I is increased. *i.e.*, at the edges. If g(x,y) is less (close to zero), the velocity decreases, and therefore, the curve evolution stops. If the the g(x,y) is not zero for smooth edges, then another gradient term of g is introduced to stop the curve evolution. As the curve re-initialization process is time consuming and complex, Kaihua Zhang, Lei Zhang proposed a Re-initialization free Level set evolution using Reaction Diffusion, which provide better results on segmenting nodules from CT scan in this work. The Level Set segmented output of Lung CT image is shown in Figure 4.

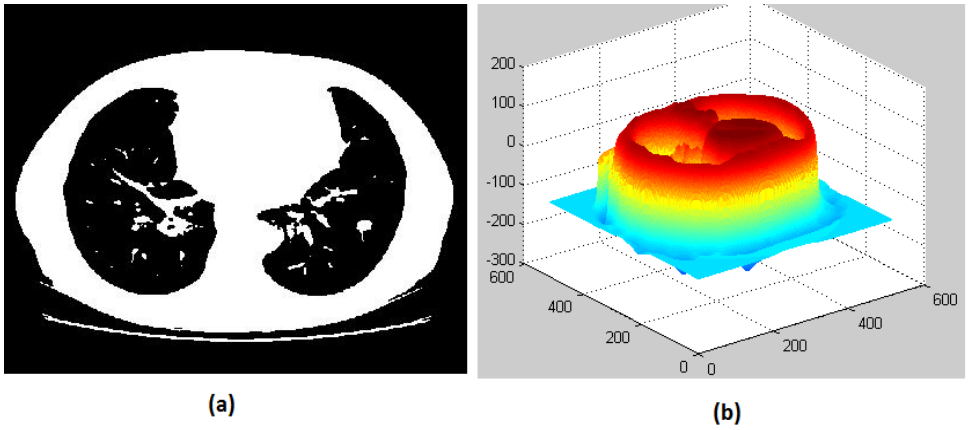

Figure 4. (a)Level Set Evolution Initial Segmentation mask, (b) Level Set Evolution Final Function

3.1. Morphological Processing to Extract Nodules

In the Figure 4 (a), the rib and heart tissue regions are segmented as white cluster along with nodules and vessels. Morphological processing is applied on the Figure 3(a), to segment the clusters within the parenchyma region of lung lobes. The following 2 step morphology is used in this work:

1. All the connected component cluster of size less than 500 pixels are removed. Therefore all the nodules and vessels are removed as show in the figure 5(a).

2. The output image of last step is subtracted from level set segmented image in Figure 4 (a). The difference between these two images are the clusters of size less than 500 pixels(nodules and vessels) and all the big structures like ribs and heart tissue regions are removed. The subtracted binary image is ANDed with the original lung CT image to segment the nodules in its original gray scale as shown in Figure 5(b)

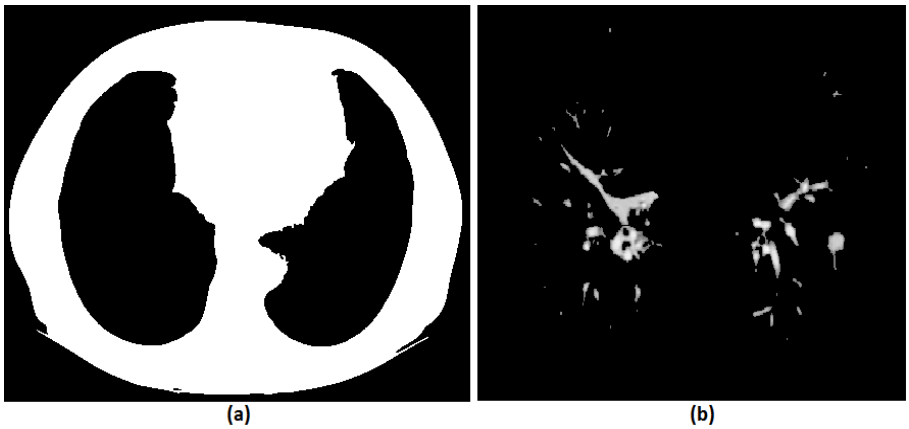

Figure 5. (a) Morphological Processing Mask, (b)Segmented Nodule Candidates

4. False Nodule Elimination

The tissue clusters segmented using level set algorithms contain both nodules and non-nodular structures. Some calcified patterns and vessels from 2D slices of CT scan segmented are actually not nodules, but these are the tissue clusters which appear like nodules. It is very essential to find the feature to discriminate non-nodules from candidate nodules.

4.1. Elimination of Vessels through 3D Centroid Variation

The tissue clusters segmented using level set algorithms contain both nodules and non-nodular structures. Some calcified patterns and vessels from 2D slices of CT scan segmented are actually not nodules, but these are the tissue clusters which appear like nodules. It is very essential to find the feature to discriminate non-nodules from candidate nodules.

The vessels which are segmented incorrectly as nodules can be eliminated by analyzing the consecutive CT slices. From one slice to another, the vessel clusters position changes drastically, whereas the actual nodule position remains relatively same. Hence by comparing the Centroid values of the segmented clusters from one slice to other, vessels can be eliminated from candidate nodules.

The algorithmic steps used for Centroid-shift analysis were as follows:

1. The Centroid value of each segmented cluster (suspected nodules) from the first CT slice was determined by using the equation

$$[Cx, Cy] = \left[\frac{\sum_{i=1}^{M}\sum_{j=1}^{N} i*f(i,j)}{\sum_{i=1}^{M}\sum_{j=1}^{N} f(i,j)}, \frac{\sum_{i=1}^{M}\sum_{j=1}^{N} j*f(i,j)}{\sum_{i=1}^{M}\sum_{j=1}^{N} f(i,j)} \right] \quad (13)$$

2. The Centroid values were computed for next 3 to 4 consecutive CT slice segmented clusters.

3. The clusters were analyzed further if the centroid shift was found to be minimum, else it has been eliminated.

4.2. Elimination of Calcifications Through Fourier DC Constant

Although the vessels that appeared like nodule in 2D analysis were removed, there were also remaining segmented objects other than the cancerous lung nodules. These non-cancerous lung nodules are known as non-nodules, calcifications or benign nodules.

Benign are formed in lung due to inflammation and scarring of lung tissue associated with bacterial or fungal infection. A type of nodule that is unlikely to be cancer is known as calcified granuloma which consists of calcium deposits.

Transforming the domain feature may be more discriminative for some cases, so in this work we also proposed to find frequency domain feature to discriminate nodules from calcifications. Discrete Fourier Transform will segregate the image regions in Low and High frequency regions, but to maintain the frequency orientation, it is essential to arrange the pixels using equation (16) before applying Fourier Transform, so that all the pixels corresponding to low frequency accumulated in the center and in various radial directions, to allow that pixels corresponding to high frequency gather at corners.

$$f(x,y) = (-1)(x+y) * g(x,y) \quad (14)$$

$$F(u,v) = \sum_{x=0}^{M-1} \sum_{y=0}^{N-1} f(x,y) * \exp[-j2\pi (\frac{mu}{M} + \frac{nv}{N})] \quad (15)$$

where u=0, 1 - - - - - M-1 and v=0,1 - - - - - N-1

The center value (M/2, N/2) of the frequency transformed image has a zero frequency value, it is also known as the DC constant, which can be a powerful feature to discriminate malignant nodules from calcifications. The frequency values at the different radii levels can also be used as a discriminative feature [19].

5. Results and Discussion

A customized histogram specification was applied on the normalized unsigned 16-bit DICOM format lung CT image. The resultant enhanced image is shown in the Figure 2. An automatic level set based segmentation algorithm is implemented in this paper to segment all the possible nodule candidates as shown in Figure 5(b). The nodule candidates less than 3mm in diameter are not have any significant information it to process it further to detect the cancerous nature of it. Hence all the nodule candidates whose size is less than 3mm are eliminated. Also the very uneven line like structure can't be the nodules, so such a structures are eliminated based on eccentricity feature. The line like structures eccentricity values deviate much from 1. The nodule candidates after applying the size and eccentricity criteria is shown in Figure 6.

Figure 6. Nodule Candidates after an Eccentricity and Size Criteria Applied

The total number of nodule candidates are reduced from 50 to 9 after applying nodule size and eccentricity criteria. The centroid value of these 9 nodule candidates are computed from the consecutive slices of CT scan. The Table 1 shows the deviation in centroid values of each nodule candidates in consecutive scan image. The centroid values of nodule candidates 1,3 and 8 remain almost constant in consecutive slices of CT image, whereas the other six nodules centroid values deviate much. Hence the 6 nodule candidates for which the centroid shift is more could be the vessels. On the other hand

further investigation need to be carried out on nodule candidate 1 3 and 8 before taking final decision on its malignancy.

Table 1. Centroid of Nodule Candidates in Consecutive CT Slice Images

	Slice 1	Slice 2	Slice 3	Slice 4	Slice 5	Slice 6	Slice 7	Slice 8	Slice 9	Slice 10	Slice 11
Nodule 1	**334 468**	**333 469**	**330 469**	**332 470**	**334 468**	**335 471**	**333 469**	**332 470**	**335 471**	-	-
Nodule 2	190 308	193 314	194 321	201 330	203 334	207 341	210 346	216 352	-	-	-
Nodule 3	**336 233**	**334 235**	**335 235**	**332 234**	**330 236**	**331 235**	**330 234**	**329 235**	**332 236**	**331 235**	
Nodule 4	-	155 285	159 287	162 287	165 289	172 294	176 298	177 305	181 308	-	-
Nodule 5	172 293	176 299	179 304	184 309	187 313	192 320	193 322	-	-	-	-
Nodule 6	-	-	-	202 300	208 303	212 308	218 313	224 317	227 320	229 323	232 325
Nodule 7	-	-	159 290	167 299	173 285	163 289	180 280	188 289	195 293	-	-
Nodule 8	-	**211 308**	**210 309**	**209 307**	**210 308**	**210 307**	**212 306**	**211 306**	**210 305**	-	-
Nodule 9	302 292	306 295	309 299	314 303	318 306	322 310	-	-	-	-	-

The nodule 1, 3 and 8 can be malignant (cancerous) nodule or just calcifications(benign). In order to discriminate malignant nodule from calcifications, the frequency domain transform analysis is carried out. The frequency spectrum of final nodule candidates 1,3 and 8 is shown in the Figure 7, and its corresponding DC constant values are tabulated in Table 2.

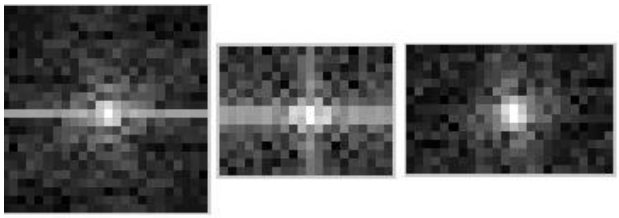

Figure 7. Frequency Spectrum of Candidate Nodules

Table 2. Frequency Spectrum DC Constant of Nodule Candidates

	DC constant
Nodule candidate 1	0.023
Nodule candidate 3	1.79
Nodule candidate 8	1.67

From Table 2, the DC constant value for nodule 1 is minimum, which reveals that nodule 1 having highly varying components in it. Nodule 3 and 8 have the DC constant value more than 1. The more value of DC constant indicates that the nodule region is homogenous and uniform. Generally the calcifications are uniform in its texture and intensity nature and malignant nodule patterns are variable ones. Therefore the proposed algorithm in this work detects nodule candidate 1 as malignant and the nodule candidates

3 and 8 as calcifications(benign). This result is matched with the radiologist report of this scan case (LIDC 60).

The algorithm developed in this work applied on 40 patient cases from LIDC database with 58 malignant nodules. This algorithm detected 55 malignant nodules correctly (True Positive) and missed 3 (False Negative) and also out of 857 false nodule candidates, 778 are eliminated correctly (True Negative) and 79 nodules are wrongly detected as malignant(False Positive). The performance measure of an algorithm implemented in this work is tabulated in Table 3. This work produced a good sensitivity and specificity of 94.8% and 93.5% respectively with an improved false positive of 1.98 per patient scan. The performance analysis of this work is compared with others in the Table 4.

Table 3. Performance Measure of Proposed Work

Statistic	Formula	Value
Sensitivity	$\frac{TP}{TP+FN}$	94.8%
Specificity	$\frac{TN}{TN+FP}$	90.8 %
Positive Likelihood Ratio	$\frac{Sensitivity}{100-Specificity}$	10.3
Negative Likelihood Ratio	$\frac{100-Sensitivity}{Specificity}$	0.057
Disease prevalence	$\frac{TP+FN}{TP+FN+TN+\ FP}$	6.33%

Table 4. Performance Comparison with Other Works

CAD system	Sensitivity in %	False Positive/Patient	Nodule Size Criteria
Zhao *et. al.,.,* (2003) [20]	84	5	2-7mm
Opfer and Wiemeker (2007) [21]	74	4	>4mm
Dehmeshki *et. al.,*.(2007) [22]	90	15.5	3-20mm
Ozekes *et. al.,* (2008) [14]	100	13.4	>5mm
Golosio *et. al.,* (2009) [23]	79	4	>4mm
Suarez Cuenca *et. al.,*.(2009) [24]	80	7.7	>4mm
Choi WJ *et. al.,*(2012) [25]	95	2.27	>1.5mm
Alilou *et. al.,* (2014) [11]	80	3.9	>4mm
Demir O *et. al.,* (2015) [12]	98	2.47	NA
Lu L *et. al.,* (2015) [13]	85	3.13	>5mm
Krishnamurthy *et. al.,*(2016) [26]	88	2.05	>3mm
Our framework	**95**	**1.98**	**>3mm**

6. Conclusion

An efficient level set evolution based segmentation followed by the 3D morphology analysis to classify the malignant lung nodules from CT scan was successfully implemented in this study. Effective pre-processing by using customized histogram specification algorithm enhanced the nodule candidates in the parenchyma region. Hence all the possible nodule candidates were segmented through LSEM algorithm. The 3D centroid analysis followed by frequency domain DC constant analysis, carried out on consecutive slices that remarkably reduced the false positives. This algorithm was applied on 40 cases having a total of 58 malignant nodules. Fifty five of 58 nodules were correctly

detected and 3 nodules were not detected. Of the other 857 segmented candidate nodules (excluding 55 malignant nodules), 778 nodules were eliminated correctly and 79 candidate nodules were incorrectly detected as malignant nodules. This work produced the better result in terms of 1.98 false positives per case with sensitivity of 94.8%.

Acknowledgment

We thank "The Cancer Imaging Archive(TCIA)" for making the LIDC database available in online for open access. We also thank Bharat scans, Chennai, India for officially providing lung CT images for our research work.

References

[1] R. Siegel, J. Ma, Z. Zou and A. Jemal, "Cancer statistics, 2014", CA: a cancer journal for clinicians, vol. 64, no. 1, **(2014)** pp. 9-29. doi: 10.3322/caac.21208.
[2] M. K. Gould, J. Donington, W. R. Lynch, P. J. Mazzone, D. E. Midthun, D. P. Naidich and R. S. Wiener, "Evaluation of individuals with pulmonary nodules: When is it lung cancer? Diagnosis and management of lung cancer", American College of Chest Physicians evidence-based clinical practice guidelines, CHEST Journal , vol. 143, no. 5, sup. l , **(2013)**, pp. e93S-e120S. doi: 10.1378/chest.12-2351.
[3] S. Chheang and K. Brown, "Lung cancer staging: clinical and radiologic perspectives", In Seminars in interventional radiology, Thieme Medical Publishers, vol. 30, no. 2, **(2013)**, pp. 99. doi: 10.1055/s-0033-1342950.
[4] B. C. Lassen, C. Jacobs, J. M. Kuhnigk, B. V. Ginneken and E. M. van Rikxoort, "Robust semi-automatic segmentation of pulmonary subsolid nodules in chest computed tomography scans", Physics in medicine and biology, vol. 60, no. 3, **(2015)**. doi: http://dx.doi.org/10.1088/0031-9155/60/3/1307.
[5] O. Gómez, J. A. González and E. F. Morales, "Image segmentation using automatic seeded region growing and instance-based learning", In Progress in pattern recognition, image analysis and applications. Springer Berlin Heidelberg, **(2007)**, pp. 192-201. ISBN:3-540-76724-X 978-3-540-76724-4.
[6] T. K. Senthil Kumar, E. N.Ganesh and R. Umamaheswari, "Automatic lung nodule segmentation using autoseed region growing with morphological masking (ARGMM) and feature extraction through complete local binary Pattern and microscopic information pattern", EuroMediterranean Biomedical Journal, vol. 10, no. 5, **(2015)**, pp. 99-119. doi: 10.3269/1970-5492.2015.10.5, 2015.
[7] T. K. S. Kumar and E. N. Ganesh, "Proposed technique for accurate detection/segmentation of lung nodules using spline wavelet techniques", International journal of biomedical science: IJBS, vol. 9, no. 1 **(2013)**, pp. 9. PMCID: PMC3644416.
[8] S. Y. Elhabian, H. A. E. Munim, S. Elshazly, A. A. Farag and M. Aboelghar, "Experiments On Sensitivity Of Template Matching For Lung Nodule Detection In Low dose Ct Scans", In Signal Processing and Information Technology, IEEE International Symposium on, **(2007)**, pp. 1029-1035, IEEE, doi: 10.1109/ISSPIT.2007.4458213.
[9] R. Nagata, T. Kawaguchi and H. Miyake, "Automated detection of lung nodules in chest radiographs using a false-positive reduction scheme based on template matching", In Biomedical Engineering and Informatics (BMEI), 2012 5th International Conference on, **(2012)**, pp. 216-223. IEEE. doi: 10.1109/BMEI.2012.6512916.
[10] H. H. Jo, H. Hong and J. M. Goo, "Pulmonary nodule registration in serial CT scans using global rib matching and nodule template matching", Computers in biology and medicine, vol. 45, **(2014)**, pp. 87-97. doi: http://dx.doi.org/10.1016/j.compbiomed.2013.10.028.
[11] M. Alilou, V. Kovalev, E. Snezhko and V. Taimouri, "A Comprehensive Framework for Automatic Detection of Pulmonary Nodules in Lung Ct Images", Image Analysis & Stereology, vol. 33, no. 1, **(2014)**, pp.13-27. doi: 10.5566/ias.v33.p13-27.
[12] Ö. Demir and A. Y. Çamurcu, "Computer-aided detection of lung nodules using outer surface features", Bio-Medical Materials and Engineering, vol. 26, **(2015)**, pp. 1213-1222. doi: 10.3233/BME-151418.
[13] L. Lu, Y. Tan, L. H. Schwartz and B. Zhao, "Hybrid detection of lung nodules on CT scan images", Medical physics 42, no. 9, **(2015)**, pp. 5042-5054. doi: http://dx.doi.org/10.1118/1.4927573.
[14] S. Ozekes, O. Osman and O. N. Ucan, "Nodule detection in a lung region that's segmented with using genetic cellular neural networks and 3D template matching with fuzzy rule based thresholding", Korean J Radiol, vol. 9, no. 1, **(2008)**, pp. 1-9.
[15] S. G. Armato III, G. McLennan, L. Bidaut, M. F. McNitt-Gray, C. R. Meyer and A. P. Reeves, "The Lung image database consortium (LIDC) and Image database resource initiative (IDRI): A completed reference database of lung nodules on CT scans", Med Phys, vol. 38, **(2011)**, pp. 915-931.
[16] C. C. Sun, "Dynamic contrast enhancement based on histogram specification", Consumer Electronics, IEEE Transactions on, vol. 51, no. 4, **(2005)**, pp. 1300-1305.
[17] M. Kass, A. Witkin and D. Terzopoulos, "Snakes: Active contour models", International Journal of Computer Vision , vol. 1, no. 4, **(1988)**, pp. 321-331.

[18] R. Kimmel, "Numerical geometry of images: Theory, algorithms, and applications", Springer Science & Business Media, **(2012)**.
[19] T. K. Senthil Kumar, E. N.Ganesh and R. Umamaheswari, "Automatic lung nodule segmentation using autoseed region growing with morphological masking (ARGMM) and feature extraction through complete local binary Pattern and microscopic information pattern", EuroMediterranean Biomedical Journal, vol. 10, no. 5, **(2015)**, pp. 99-119. DOI: 10.3269/1970-5492.2015.10.5.
[20] B. Zhao, "Automatic detection of small lung nodules on CT utilizing a local density maximum algorithm", Journal Appl Clin Med Phys, vol. 4, no. 3, **(2003)**, pp. 248-260.
[21] R. Opfer and R. Wiemker, "Performance analysis for computer-aided lung nodule detection on LIDC data", Medical Imaging, International Society for Optics and Photonics, **(2007)**, pp. 65151C-65151C.
[22] J. Dehmeshki, X. Ye, X. Lin, M. Valdivieso and H. Amin, "Automated detection of lung nodules in CT images using shape-based genetic algorithm. Comput Med Imag Grap, vol. 31, no. 6, **(2007)**, pp. 408-417.
[23] B. Golosio, "A novel multithreshold method for nodule detection in lung CT", Med Phys, vol. 36, no. 8, **(2009)**, pp. 3607-3618.
[24] J. J. Suárez-Cuenca, P. G. Tahoces, M. Souto, M. J. Lado, M. R. Jardin, J. Remy and J. J. Vidal, "Application of the iris filter for automatic detection of pulmonary nodules on computed tomography images", Comput Biol Med, vol. 39, no. 10, **(2009)**, pp. 921-933.
[25] W. J. Choi and T. S. Choi, "Automated pulmonary nodule detection system in computed tomography images: A hierarchical block classification approach", Entropy, vol. 15, no. 2, **(2013)**, pp. 507-523
[26] S. Krishnamurthy, G. Narasimhan and U. Rengasamy, "Three-dimensional lung nodule segmentation and shape variance analysis to detect lung cancer with reduced false positives", Proceedings of the Institution of Mechanical Engineers, Part H: Journal of Engineering in Medicine, vol. 230, no. 1, **(2016)**, pp. 58-70.

